Int J Thermophys (2008) 29:944–957
DOI 10.1007/s10765-007-0334-4

# Investigation of TiC–C Eutectic and WC–C Peritectic High-Temperature Fixed Points

**Naohiko Sasajima · Yoshiro Yamada**

Published online: 20 February 2008


**Abstract** TiC–C eutectic (2,761°C) and WC–C peritectic (2,749°C) fixed points were investigated to compare their potential as high-temperature thermometric reference points. Two TiC–C and three WC–C fixed-point cells were constructed, and the melting and freezing plateaux were evaluated by means of radiation thermometry. The repeatability of the TiC–C eutectic within a day was 60 mK with a melting range roughly 200 mK. The repeatability of the melting temperature of the WC–C peritectic within 1 day was 17 mK with a melting range of ∼70 mK. The repeatability of the freezing temperature of the WC–C peritectic was 21 mK with a freezing range less than 20 mK. One of the TiC–C cells was constructed from a TiC and graphite powder mixture. The filling showed the reaction with the graphite crucible was suppressed and the ingot contained less voids, although the lack of high-purity TiC powder poses a problem. The WC–C cells were easily constructed, like metal–carbon eutectic cells, without any evident reaction with the crucible. From these results, it is concluded that the WC–C peritectic has more potential than the TiC–C eutectic as a high-temperature reference point. The investigation of the purification of the TiC–C cell during filling and the plateau observation are also reported.

**Keywords** Eutectic · High temperatures · Peritectic · Radiation thermometer · Temperature standards · Titanium carbide · Tungsten carbide

N. Sasajima (✉) · Y. Yamada
Radiation Thermometry Section, National Metrology Institute of Japan (NMIJ), AIST,
1-1-1 Umezono, Tsukuba, Ibaraki 305-8563, Japan
e-mail: n.sasajima@aist.go.jp

## 1 Introduction

Many national metrology institutes are currently developing high-temperature fixed points beyond the copper point (1,084.62°C) based on metal–carbon (M–C) and metal carbide–carbon (MC–C) eutectics to reduce the uncertainty of temperature scale realization at high temperatures [1,2]. Moreover, MC–C eutectics are promising candidates for radiance and irradiance standards in photometry and radiometry because they are located above 2,500°C and are available up to 3,185°C (HfC–C) [3]. In a previous investigation by the authors on the TiC–C eutectic fixed point, the melting plateaux showed repeatability of 20 mK with a melting range of roughly 1.5 K. The freezing plateaux showed a sharp peak after recovering from the supercool, followed by a gently sloped curve, a shape that has not been encountered in M–C eutectics [4]. However, this result was obtained by measurements of only one cell and from three melting and freezing cycles. Other investigations of the TiC–C eutectic fixed point followed, though mainly to utilize the fixed point to reduce the uncertainty of photometric and radiometric measurements [3,5]. These studies showed that, even though (in some cases) a repeatability of 50 mK was observed for one cell or agreement of 200 mK was achieved between different cells, the results were not always reproducible and seemed to depend on the furnace conditions and on the uniformity of the cell ingot form [3,5,6]: TiC–C cells sometime show large voids in the ingot, resulting in poor melting plateaux [5]. Although the performance of high-temperature furnace facilities has been improved in the meantime [7], due to the difficulty of the cell construction and the lack of means to improve the robustness of the cells, which are prone to breakage, development of MC–C eutectic fixed points is slow compared to M–C eutectics, and detailed investigations of the plateau shape of MC–C eutectics have not yet been conducted.

Recently, in addition to M(C)–C eutectics, the authors reported new high-temperature MC–C peritectic fixed-points: $Mn_7C_3$–C (1,331°C), $Cr_3C_2$–C (1,826°C), and WC–C (2,749°C) [8]. These fixed points involve a reaction among the same three phases as the MC–C eutectic reaction (MC, C, and the liquid phases) and therefore, they too could be realized without being contaminated by the graphite from the crucible. A detailed explanation of the peritectic reaction is described in [9]. In [8], the peritectics showed melting-plateau repeatability of 20 mK and a melting range of roughly 100 mK, although the nominal purities of the metals used in that study were 99.95%, 99.9%, and 99.99% for Mn, Cr, and W, respectively. To evaluate their performance as fixed points and to understand the mechanism of the peritectic reaction, the authors have initiated an investigation of the MC–C peritectic systems; the filling procedure and microstructure analysis of the $Cr_3C_2$–C peritectic system, performed in relation to the observed melting and freezing behavior, are reported in another paper in these proceedings [9], and the melting plateau's dependence on material purity, thermal history, and melting rate of the $Cr_3C_2$–C peritectic point is reported in a second paper [10].

In this article, we describe the experimental investigation of the WC–C peritectic fixed point in conjunction with that of the TiC–C eutectic point, a fixed point with a similar melting temperature, with the aim to understand the differences between the two systems, and to compare their suitability as high-temperature reference points.

In the previous investigation, not only the melting plateau but also the freezing plateau of the WC–C peritectic point was flat [8]. However, this result was obtained by measurement of one sintered porous-ingot cell and from only three melting and freezing cycles. In the current investigation, two TiC–C and three WC–C fixed-point cells were constructed by different procedures, and their performance, sensitivity against impurity, and ease-of-cell construction were evaluated by means of a radiation thermometer.

## 2 Experimental

### 2.1 Construction of Fixed-Point Cells

The graphite crucibles containing the TiC–C eutectic and WC–C peritectic fixed-point materials were the same, with an outer diameter of 24 mm and a length of 45 mm. The blackbody cavity has an aperture diameter of 3 mm, a cavity length of 34 mm, and a conical bottom with an apex angle of 120°. The wall thickness of the cavity is 2 mm. The graphite crucible of 99.9995% nominal purity was machined and purified by the manufacturer. Effective emissivities of the cavities are estimated to be 0.9997. High-purity graphite powder of 99.9999% nominal purity (supplier: Alfa Aesar) was used in the mixture of all fillings.

#### *2.1.1 Construction of TiC–C Eutectic-Point Cells*

The filling of the TiC–C eutectic-point cells is complicated for two reasons. Firstly, the eutectic composition is at 27% mass fraction of carbon, which is a very high carbon concentration if one considers that this value is less than 3% for most M–C eutectics. The large amount of carbon required for the eutectic reaction would result in a significant reaction with the crucible wall wherever the mixture lacks carbon, and in the formation of a porous ingot structure where the carbon is in excess (non-uniform mixing of the powder would form a nonuniform ingot). Secondly, the binary phase diagram of the Ti-C system indicates that Ti and C react to form a eutectic of Ti-TiC at 1,647°C, and the melting of pure titanium occurs at 1,670°C [11], that is, all of the titanium powder reacts heavily with the graphite powder and the graphite crucible to make TiC slightly below 1,700°C. This fact is supported by the observation of sudden heat generation around this temperature during the heating phase of the filling process. The structure formed at this stage is found to be porous or with large voids, for the TiC has a melting temperature higher than 3,000°C and therefore does not flow at 1,700°C. At 2,761°C, the generated TiC reacts with graphite to form a molten alloy on heating which then forms the TiC–C eutectic on cooling. The formation of large voids in the final ingot may be attributed to this two-step reaction involving an intermediate porous-ingot structure.

In this study, a novel filling technique was devised to overcome these difficulties. One cell was prepared starting from TiC powder of 99.5% nominal purity (supplier: Furuuchi Chemical Co.). The powder was mixed with graphite powder at 8.5% mass fraction of the latter, so that the total carbon mass fraction becomes 27%. Another cell was prepared by the conventional filling method starting from titanium powder

of 99.99% nominal purity (supplier: Alfa Aesar). Both cells contain a sacrificial inner graphite sleeve that protects the outer wall. They were placed in a BB3500YY furnace oriented for vertical operation, as described in Sect. 2.2, and raised to a temperature above the eutectic temperature in an Ar atmosphere. They were then cooled to room temperature and more powder mixture was added. The process was repeated until the crucibles were filled. A TiC–C cell with a uniform ingot was easily constructed using TiC powder, and no damage to the crucible was observed from a reaction during filling. The TiC–C cells filled using TiC powder and titanium powder were labeled TiC-1 and TiC-2, respectively. The resulting masses of the eutectic samples were 14.0 g and 12.8 g for TiC-1 and TiC-2, respectively.

#### *2.1.2 Construction of WC–C Cells*

Three WC–C peritectic cells were constructed using different procedures: two cells (6SS-N1 and 6SS-N2) were prepared from large-grain-size tungsten powder of 99.9999% nominal purity (supplier: Nikko Metals Co., Ltd), and another cell (6SS-N3) was prepared from tungsten powder of 99.99% nominal purity (supplier: Kojundo Chemical Laboratories Co., Ltd) which is the same product, but a different lot, as used in the previous investigation [8]. All cells contained two layers of graphite cloth material ("C/C sheet" TCC-019, manufactured by Toyo Tanso Co. Ltd) around the ingot to improve the temperature uniformity of the cell [12]; 6SS-N2 and 6SS-N3 cells additionally used two layers of a 0.1 mm thick purified graphite paper between the C/C sheet and the ingot to prevent absorption of the molten alloy by the C/C sheet. The tungsten powder was mixed with graphite powder at the WC composition of 6.0% mass fraction of carbon (∼50% atomic fraction of carbon). The graphite crucible was filled with the mixture, and the cell was then placed in the vertical BB3500YY furnace. The furnace temperature was raised above the WC–C peritectic temperature in an Ar atmosphere without the sintering step, with the intention to form a non-porous ingot, which is different from the previous investigation where a porous ingot was made [8]. All cells were easily constructed without significant reaction with the crucible, C/C sheet, and graphite paper, similar to our M–C eutectic cells. The mass of the metal/carbon mixture was 36.26 g, 35.65 g, and 24.13 g for 6SS-N1, 6SS-N2, and 6SS-N3, respectively. The small amount of metal filled in 6SS-N3 may be explained by the fineness of the tungsten powder used, which tends to form a porous sintered ingot.

### 2.2 Furnace and Radiation Thermometer

A BB3500YY furnace with a heater tube of 47 mm inner diameter was used in all fillings and investigations. The heater tube consists of a stack of pyrolytic graphite rings that are pressed together between electrodes by means of a steel spring that pushes them against the front electrode. For the filling of the cells, the furnace was oriented for vertical operation. For the plateau observations, the furnace was operated horizontally with insertion of a cell holder composed of a graphite flange and a C/C composite tube of 27 mm inner diameter; the holder and the cell are thus heated by

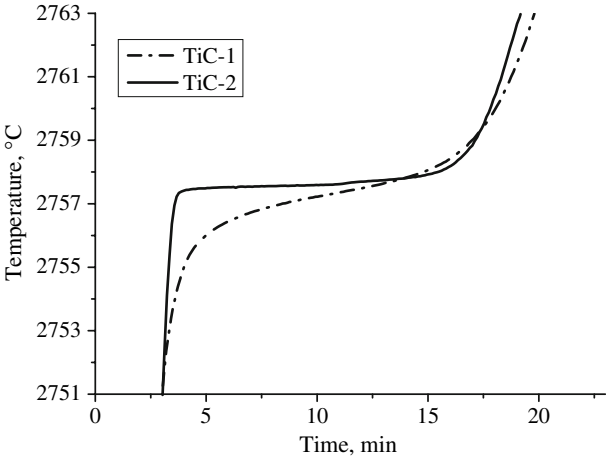


**Fig. 1** Comparison of the melting plateaux of the TiC-1 and TiC-2 cells. Melting plateaux were realized at the same furnace-temperature setting of $\Delta T = +20\,\mathrm{K}$

radiation. The axial temperature distribution can be optimized by ordering the ring elements based on their individual electrical resistance. Details of the furnace and its temperature distribution optimization are described in [7]. The front window of the furnace was opened during the measurements by use of a purge unit; the inside of the furnace is additionally purged by a steady flow of Ar gas from the back to the front.

The melting and freezing plateaux were observed by two linear pyrometer 3 (LP3) radiation thermometers (manufactured by KE) with an operating wavelength of 650 nm. The target diameter is ∼0.9 mm at a target distance of 700 mm. They were not calibrated for the measurements, and the temperature values appearing in this article are only for reference.

## 3 Results

### 3.1 TiC–C Eutectic Cells

#### *3.1.1 Comparison between TiC-1 and TiC-2 Cells*

Melting and freezing plateaux of the samples were induced by offsetting the furnace temperature $\Delta T$ with respect to the nominal eutectic transition temperature. The inflection point of the melting plateau was taken as the melting temperature, and the slope at the inflection point multiplied by the plateau duration was taken as the melting range.

Figure 1 compares the melting curves of the TiC-1 and TiC-2 cells. The furnace-temperature settings for both melting plateaux were the same ($\Delta T = +20\,\mathrm{K}$). The TiC-1 cell showed a larger melting range and lower melting temperature compared to the TiC-2 cell; the melting ranges were roughly 2.0 K and 200 mK for TiC-1 and TiC-2, respectively. Table 1 summarizes the analysis results in terms of mass fraction (ppm)

**Table 1** Results of metallic impurity analysis by GD-MS

| | TiC powder (ppm mass) | TiC-1 (ppm mass) | Ti powder (ppm mass) | TiC-2 (ppm mass) |
|---|---|---|---|---|
| B | 150 | 150 | 0.64 | 1.2 |
| Na | 1.5 | 1.3 | 6.5 | 0.31 |
| Mg | 1.4 | 0.11 | 0.54 | 0.07 |
| Al | 4,500 | 5.6 | 7.4 | 0.33 |
| Si | 44 | 4.7 | 7.3 | 1.5 |
| S | 27 | 1.8 | 2.4 | 0.29 |
| Cl | 8.5 | 14 | 20 | 2.4 |
| Ca | 2.2 | 2.4 | 3.5 | 1.5 |
| V | 180 | 98 | 0.22 | 2.5 |
| Cr | 120 | 18 | 3 | 1.1 |
| Mn | 8.5 | <0.05 | 0.31 | <0.05 |
| Fe | 870 | 2.7 | 20 | 0.77 |
| Co | 340 | <0.05 | 0.86 | <0.05 |
| Ni | 29 | 0.53 | 5.6 | 0.13 |
| Cu | 5.2 | 3.3 | 20 | 5.6 |
| As | 1.4 | <0.5 | <0.5 | <0.5 |
| Zr | 660 | 220 | 1.2 | 0.67 |
| Nb | 610 | 270 | <1 | <1 |
| Mo | 12 | 4.5 | <0.5 | 2.5 |
| Hf | 16 | 5.2 | <0.05 | 0.09 |
| W | 2,800 | 1,100 | 0.38 | <0.1 |
| Pt | 1.5 | <0.1 | <0.1 | <0.1 |
| Pb | 2.2 | 3.2 | 2.1 | 1.5 |
| Total | 10,390.4 | 1,905.3 | 102.0 | 22.5 |

for the metallic impurities detected by glow discharge mass spectrometry (GD-MS). Samples for the analysis were prepared using an open crucible and the same filling procedure described in Sect. 2.1.1. Although evaporation of impurities from the molten alloy during filling is observed in both cells, the TiC-1 cell retains higher impurity content consistent with its lower-purity starting material.

### *3.1.2 Plateau Observation of TiC-2 Cells*

The freezing plateaux of both TiC–C cells showed a sharp peak after recovering from the supercool followed by a gently sloped curve, as was observed in the previous investigation [4]. The peak temperature of the freezing plateau was higher than the melting temperature. For the TiC-2 cell, 22 melting and freezing cycles were realized by changing the furnace-temperature offset from 10 to 30 K with respect to the eutectic

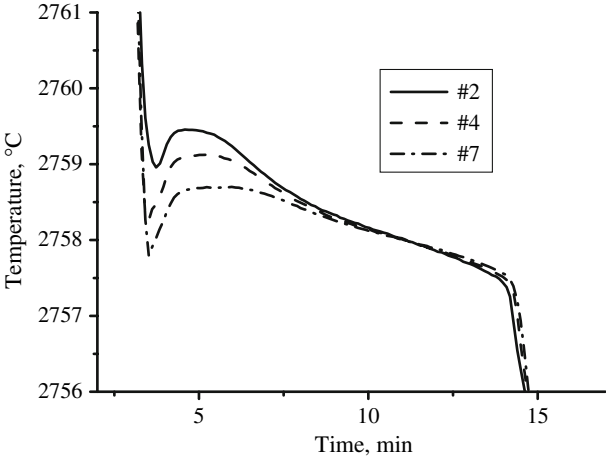


**Fig. 2** Freezing plateaux of the TiC-2 cell. All freezes were realized by changing the furnace-temperature setting from $\Delta T = +20\,\mathrm{K}$ to $\Delta T = -20\,\mathrm{K}$

temperature. In Fig. 2, three examples of the freezing plateaux of the TiC-2 cell are shown. ID numbers appearing in the figure represent the order of the melting/freezing cycles counting from the first observation. These three freezes were realized by the same stepwise change in the furnace-temperature setting from $\Delta T = +20\,\mathrm{K}$ to $\Delta T = -20\,\mathrm{K}$. It may be discerned from the figure that the peak temperature of the freezing plateau became lower and lower with each successive melting/freezing cycle. On the other hand, the melting temperature became higher and higher with each cycle, as illustrated in Fig. 3, and the temperature difference between melt and freeze became smaller—it was reduced from 2.2°C for the first cycle to less than 0.3°C for the 22nd, although the peak freezing temperature is still higher than the melting temperature. For the TiC-2, the repeatability of the eight melting plateaux within a day was 60 mK under the same melting condition.

## 3.2 WC–C Peritectic Cells

### *3.2.1 Plateau Observation of WC–C Peritectic Point*

Figure 4 compares the WC–C peritectic melting plateaux of the 6SS-N1, N2, and N3 cells obtained with a furnace temperature setting of $\Delta T = +20\,\mathrm{K}$ with respect to the peritectic temperature. The difference in the plateau duration apparent in the figure corresponds to the difference in ingot mass contained in the cells, combined with the existence of the extra graphite paper that acts as a thermal insulator to slow the melting process. The melting ranges of 6SS-N1, 6SS-N2, and 6SS-N3 are approximately 160 mK, 300 mK, and 70 mK, respectively. The repeatability of 10 melting plateaux of the 6SS-N3 cell within a day is 17 mK. The difference in plateau quality cannot be related to the nominal metal purity, and needs further investigation.

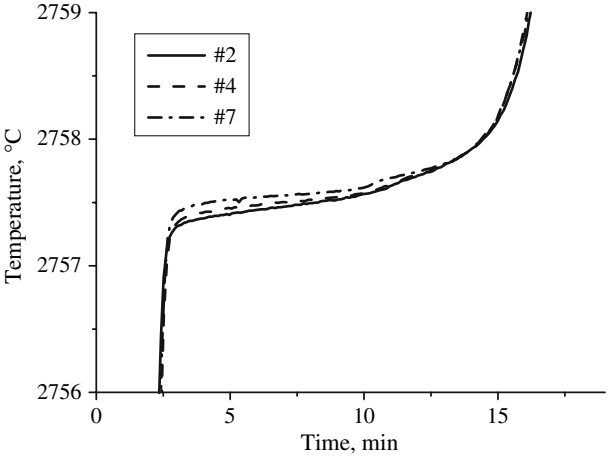


**Fig. 3** Melting plateaux of the TiC-2 cell. All melts were realized by changing the furnace-temperature setting from $\Delta T = -20\,\mathrm{K}$ to $\Delta T = +20\,\mathrm{K}$

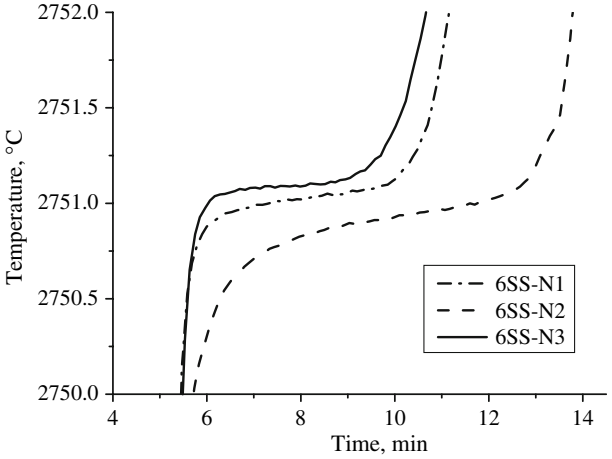


**Fig. 4** Comparison of the melting plateaux of 6SS-N1, N2 and N3 cells for WC–C peritectic point. All plateaux were realized by the same furnace temperature setting of $\Delta T = +20\,\mathrm{K}$

Figure 5 shows all melting plateaux for the 6SS-N3 cell. Ten melt/freeze cycles of the WC–C peritectic point were measured in a single day. For the melt, all plateaux were realized at $\Delta T = +20\,\mathrm{K}$. For the freeze, the first four plateaux were obtained at $\Delta T = -20\,\mathrm{K}$. After that, it became necessary to realize the freeze at $\Delta T = -30\,\mathrm{K}$ or lower to further force-cooling in order to overcome the supercool that became deeper with repeated cycles. In Fig. 6, the first four freezing plateaux of the 6SS-N3 cell induced with $\Delta T = -20\,\mathrm{K}$ are shown. The repeatability of the freezing temperature, taken as the peak temperature of the smoothed curve, for the freezes induced with both $\Delta T = -20\,\mathrm{K}$ and $-30\,\mathrm{K}$ was 21 mK, with a freezing range of less than

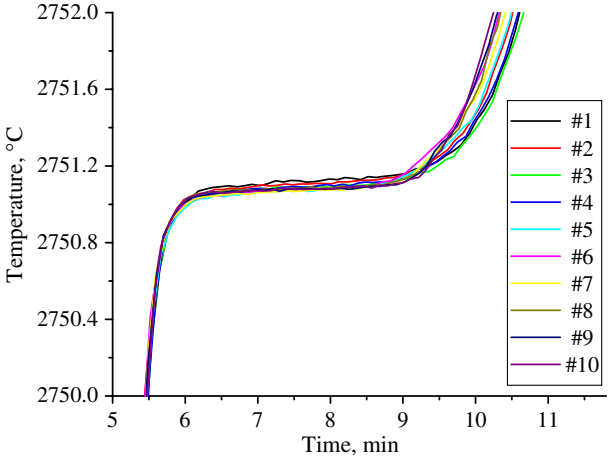


**Fig. 5** Series of melting plateaux for the 6SS-N3 cell at the WC–C peritectic point, all with $\Delta T = +20\,\mathrm{K}$

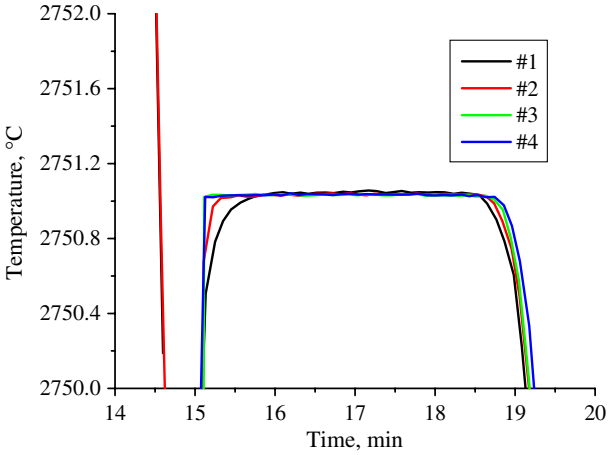


**Fig. 6** Series of freezing plateaux for the 6SS-N3 cell at the WC–C peritectic point, all with $\Delta T = -20\,\mathrm{K}$

20 mK. The repeatability of the first four freezing plateaux shown in Fig. 4 is apparently better. However, one cannot conclude from this whether or not there is a dependence of the freezing temperature on the freeze rate, for we cannot exclude the drift of the thermometer, which would make measurements extending over a longer time period appear less repeatable; one should note that the repeatability includes the possible drift of the radiation thermometer that is exposed to strong thermal radiation during the measurement of such a high temperature. The effect of the preceding freeze on the melting plateau was not investigated because of the difficulty in controlling the preceding freezing condition due to the deep supercool.

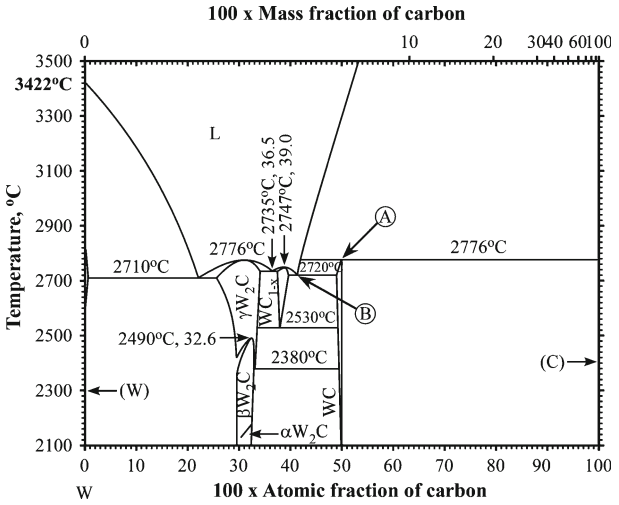


**Fig. 7** W–C binary phase diagram (original diagram taken from [11]): A: WC–C peritectic point, B: $WC_{1-x}$–WC eutectic point

### *3.2.2 Plateau Observation of $WC_{1-x}$–WC Eutectic Point*

In the Cr–C system, both the $Cr_3C_2$–C peritectic point (1,826°C) and the $Cr_7C_3$–$Cr_3C_2$ eutectic point (1,742°C) are realized in one cell [9,10]. In the W–C binary system, the $WC_{1-x}$–WC eutectic point also exists just below the peritectic point, as shown in Fig. 7. Therefore, the observation of the $WC_{1-x}$–WC eutectic point was conducted with the 6SS-N1 cell. In contrast to the $Cr_7C_3-Cr_3C_2$ eutectic-point cell constructed from chromium with a nominal purity of 99.99%, which showed a plateau duration of more than 2 min and a melting range of roughly 410 mK for a furnace setting of $\Delta T = +20$ K relative to the eutectic point, the duration of the $WC_{1-x}$–WC eutectic melting in the same design cell is less than 1 min with a large melting range of roughly 830 mK, even with a furnace temperature setting of $\Delta T = +8$ K.

## 4 Discussion

### 4.1 Filling of the Cells

In this study, a TiC–C cell with a uniform ingot was easily constructed from a TiC powder and graphite powder mixture. This is thought to be due to the small amount of graphite in the powder mixture and/or the absence of the reaction around 1,700°C to form TiC. Although, to the authors' knowledge, the highest purity of TiC powder commercially available is 99.9%, the method can become a reliable means of producing cells of high quality if high-purity TiC powder can be obtained.

WC–C cells were easily constructed without any apparent severe reaction with the graphite crucible. The small amount of graphite in WC–C, 6% in mass, is much closer to that of M–C eutectics than that of TiC–C, at 27%, and therefore the similarity to the

former in the method of filling is not so surprising. Furthermore, the phase diagram of the W–C system shows that the melting temperature of tungsten, at 3,422°C, is almost 700°C above the lowest temperature for the liquid phase at the eutectic point between W and $\gamma W_2C$ at 2,710°C (Fig. 7), only 40°C lower than the measured WC–C peritectic point, and no carbide phases of high melting temperature exist. This is in contrast to the Ti–C system, for which both the titanium melting temperature and the lowest temperature of the liquid phase exist 1,000°C below the TiC–C eutectic point, while TiC has a melting temperature exceeding 3,000°C. This means the reaction between W and C can be expected to be much slower than between Ti and C until the peritectic point is approached, where a rapid reaction occurs to form the liquid phase. This might be the main reason why the WC–C cell is easily constructed. For Ti and C, on the other hand, a rapid reaction occurring around 1,700°C forms the solid TiC phase in a porous state or with large voids that tends to remain after the TiC–C eutectic melts.

For the $Cr_3C_2$–C peritectic point, the molten metal was seen to wet and spread along the graphite crucible surface leaving large voids in the ingot, indicating a low surface energy of the molten metal [9]. This was not observed for the WC–C peritectic, which also contributed to the ease of filling.

### 4.2 TiC–C Eutectic-Point Plateaux—Purification during Filling and in Use

It was reported that certain impurities in Ti powder could be drastically reduced or eliminated after smelting with graphite powder in an argon atmosphere [13]. Impurity analysis (Table 1) has verified that the purity of the TiC–C ingot (TiC-2) constructed from Ti powder of 99.99% nominal purity became 99.998%. However, the purity of the TiC–C ingot (TiC-1) constructed from TiC powder of 99% nominal purity could only be purified to 99.8%. It is suspected that, due to the high impurity concentration, the lack of time in the molten state is the cause, although one cannot exclude the possibility that impurities in the TiC powder behave differently from those in Ti powder.

It is natural to think that the peak shift in the freezing plateau of Fig. 2 is due to the purification of the TiC–C ingot during the measurements; impurities evaporate from the molten alloy during melting/freezing cycles, resulting in increasingly flatter plateaux. If so, this indicates that the purification described in [13] is in progress, although the time required in the molten state for complete purification may be impractically long. Further investigation with cells constructed from higher-purity TiC powder is therefore of interest. The study of the purification process is of interest for application to other higher-temperature fixed points such as ZrC–C and HfC–C.

### 4.3 WC–C Peritectic Plateaux: Melting/Freezing Range

Although the nominal purity of starting material used in the 6SS-N1 and N2 cells is better than that used in the 6SS-N3 cell, Fig. 4 seems to indicate that the purity of the WC–C ingot in the 6SS-N3 cell is better than that of the other cells. However, although 6SS-N1 and N2 are both made from the same material, the two show distinctively

different plateaux. Unresolved influencing factors other than impurities or contamination during the filling process might be responsible. Another difference between 6SS-N3 and the other two cells is that it appears to contain more pores, which is reflected in the reduced ingot mass. The porous structure of 6SS-N3, which most likely relates to an increased concentration of graphite surfaces, might influence the plateau shape.

In this study, not only flat melting plateaux but also flat freezing plateaux were observed for WC–C. This has neither been observed for any of the M(C)–C eutectics nor for the $Cr_3C_2$–C peritectic points. Although it is too early to make definite statements on the cause, some remarks should be given on possible reasons for this to happen.

One possibility is the lack of a surface energy term related to the solid–liquid interface curvature. The classical theory of the peritectic reaction assumes that the peritectic phase (in this case, WC) forms on the surface of the primary phase (graphite) and grows by thickening. The structure and the plateau behavior observed for the Cr–C system seems to conform to this theory [9,10]. Many directional solidification studies indicate, however, that very often the primary $\alpha$-phase forms cells or dendrites, while the peritectic $\beta$-phase forms in the interdendritic or intercellular region, depending on the freezing condition and on the material condition [14–16]. Furthermore, in most peritectic systems, the peritectic $\beta$-phase can form directly from the liquid [17]. Therefore, it is of interest to observe the structure of the WC–C peritectic reaction, to see whether there are fine curvatures at the solid–liquid interface that can cause an undercooling of the freezing temperature, as in the case of M(C)–C eutectics.

Secondly, the classical theory states that the growth of the secondary phase has to involve diffusion through the envelope, which rarely goes to completion because solid-state diffusion is quite slow. This has been confirmed by the fact that the liquid state remains after the peritectic freezing plateau appears completed for the Cr–C system [9,10]. However, the situation may be different for the W–C system. When one compares the binary phase diagram of W–C (Fig. 7) with that of Cr–C, one notices that, unlike Cr–C, for W–C the liquidus slope hardly differs above and below the peritectic point. Above the peritectic point, the liquidus gives the equilibrium between the liquid and the primary phase (graphite), and below, the equilibrium is between the liquid and the secondary phase (WC). The small difference in the two slopes indicates that, even below the peritectic point, the graphite primary phase is still close to equilibrium with the liquid, and graphite surfaces can exist in contact with liquid without being enveloped by the WC secondary phase. This has been shown for Cu–Sn in [17], where cellular secondary phase structures are seen to grow perpendicular to the primary phase surface, leaving intercellular channels of liquid in contact with the primary phase. In such structures, diffusion does not necessarily take place in the solid phase but can occur in the liquid phase along the channel.

As is apparent from Fig. 5, the plateau duration of the WC–C peritectic point stays unchanged when the melt with $\Delta T = +20\,\mathrm{K}$ was repeated, which is in contrast to the plateau duration of the $Cr_3C_2$–C peritectic point, which became shorter and shorter with simple repetition [10]. This observation is in accord with the above assumption of rapid diffusion in the liquid enabling completion of the freeze.

A third possibility is the abundance of graphite surfaces in the liquid, where the peritectic reaction can occur. The powder mixture initially filled was at the WC composition. When the WC melts at the peritectic point, the liquid phase and graphite form, and the ratio of the two is given by the "lever rule." Comparison of phase diagrams indicates that more graphite is generated for WC than for $Cr_3C_2$.

### 4.4 $WC_{1-x}$–WC Eutectic Plateaux

The eutectic melting plateau of $WC_{1-x}$–WC has a large melting range and a short duration compared to that of the $Cr_7C_3$–$Cr_3C_2$ eutectic point. The short duration of the WC–C eutectic plateau indicates that, unlike the $Cr_3C_2$–C peritectic point, the WC–C peritectic reaction was almost completed and little liquid phase remained, as explained above.

## 5 Conclusion

TiC–C eutectic and WC–C peritectic fixed points were investigated to compare their performance and suitability as high-temperature reference points. The results show that the WC–C peritectic has a potential advantage for practical use: the repeatability of the melting plateaux was 17 mK with a melting range of ∼70 mK, which is similar to, or better than, the performance of the best M–C eutectics. Easy construction of the WC–C cell, similar to that of M–C eutectic cells, is also an advantage. However, the plateau quality differed from cell to cell. Further study is needed to understand the influence of impurities on the melting process by using different materials, impurity analyses, and thermodynamic calculations.

The freezing plateaux of the WC–C peritectic also showed high performance; the repeatability was 21 mK with a freezing range of less than 20 mK. The main problem in using the freezing plateau is the occurrence of deep supercools. If this is overcome, the freeze might be used as a temperature reference point.

Since the quality of the melting plateau of the $WC_{1-x}$–WC eutectic is poor and the temperature difference between the WC–C peritectic and the $WC_{1-x}$–WC eutectic is merely 29°C, the introduction of the $WC_{1-x}$–WC eutectic point does not seem to bring about additional advantage.

By using TiC powder, a TiC–C cell with a uniform ingot was easily constructed. However, we need to obtain high-purity TiC powder. Although the performance of the TiC–C cell is inferior to the WC–C peritectic, the repeatability of the melting plateau of 60 mK with a melting range of 200 mK is good enough for practical use. Furthermore, the filling technique of TiC–C can be applied to the ZrC–C (2,883°C) and HfC–C (3,185°C) eutectic points because these phase diagrams are similar to the Ti–C system.

Further investigations of the MC–C eutectic and peritectic phase transitions are envisaged to confirm the reproducibility between different cells, the dependence on impurity, the effect of preceding freezing rate and melting rate, structural effects, as well as sensitivity to the filling method.

**Acknowledgment** A part of this study was financially supported by the Budget for Nuclear Research of the Ministry of Education, Culture, Sports, Science and Technology, based on the screening and counseling by the Atomic Energy Commission.

## References

1. Y. Yamada, MAPAN-J. Metrol. Soc. India **20**, 183 (2005)
2. E.R. Woolliams, G. Machin, D.H. Lowe, R. Winkler, Metrologia **43**, R11 (2006)
3. V. Sapritsky, B. Khlevnoy, V. Khromchenko, S. Ogarev, M. Samoylov, Yu. Pikalev, in *Temperature: Its Measurement and Control in Science and Industry*, vol. 7, ed. by D.C. Ripple (AIP, New York, 2003), pp. 273–277
4. N. Sasajima, Y. Yamada, F. Sakuma, in *Temperature: Its Measurement and Control in Science and Industry*, vol. 7, ed. by D.C. Ripple (AIP, New York, 2003), pp. 279–284
5. M. Sakharov, B. Khlevnoy, V. Sapritsky, M. Samoylov, S. Ogarev, in *Proceedings of TEMPMEKO 2004, 9th International Symposium on Temperature and Thermal Measurements in Industry and Science*, ed. by D. Zvizdić, L.G. Bermanec, T. Veliki, T. Stašić (FSB/LPM, Zagreb, Croatia, 2004), pp. 319–324
6. N. Sasajima, M. Sakharov, B. Khlevnoy, Y. Yamada, M. Samoylov, S. Ogarev, P. Bloembergen, V. Sapritsky, in *Proceedings of TEMPMEKO 2004, 9th International Symposium on Temperature and Thermal Measurements in Industry and Science*, ed. by D. Zvizdić, L.G. Bermanec, T. Veliki, T. Stašić (FSB/LPM, Zagreb, Croatia, 2004), pp. 1107–1115
7. B. Khlevnoy, M. Sakharov, S. Ogarev, V. Sapritsky, Y. Yamada, K. Anhalt, in *Proceedings of TEMPMEKO 2007*, *Int. J. Thermophys.,* doi:10.1007/s10765-007-0347-z
8. Y. Yamada, Y. Wang, N. Sasajima, Metrologia **43**, L23 (2006)
9. Y. Yamada, Y. Wang, W. Zheng, N. Sasajima, in *Proceedings of TEMPMEKO 2007, Int. J. Thermophys.*, doi:10.1007/s10765-007-0297-5
10. W. Zheng, Y. Yamada, Y. Wang, in *Proceedings of TEMPMEKO 2007*, *Int. J. Thermophys.,* doi:10.1007/s10765-008-0381-5
11. Desk Handbook, *Phase Diagrams for Binary Alloys*, ed. by H. Okamoto (ASM Int., Materials Park, Ohio, 2000)
12. Y. Yamada, B. Khlevnoy, Y. Wang, T. Wang, K. Anhalt, Metrologia **43**, S140 (2006)
13. A. Bourdakin, M. Sakharov, B. Khlevnoy, S. Ogarev, V. Sapritsky, in *Proceedings of TEMPMEKO 2007* (to be published in *Int. J. Thermophys.*)
14. M. Vandyoussefi, H.W. Kerr, W. Kurz, Acta Mater. **48**, 2297 (2000)
15. S. Dobler, T.S. Lo, M. Plapp, A. Karma, W. Kurz, Acta Materialia **52**, 2795 (2004)
16. T.A. Lograsso, B.C. Fuh, R. Trivedi, Metall. Mater. Trans. A **36A**, 1287 (2005)
17. D.H. St. John, Acta Metall. Mater. **38**, 631 (1990)